Published in final edited form as:
Nano Lett. 2010 January ; 10(1): 85–91. doi:10.1021/nl902865v.

"Smart" Diblock Copolymers as Templates for Magnetic-Core Gold-Shell Nanoparticle Synthesis

Michael A. Nash, **James J. Lai**, **Allan S. Hoffman**, **Paul Yager**, and **Patrick S. Stayton***
Department of Bioengineering, University of Washington, Seattle, WA 98195

Abstract

We report a new strategy for synthesizing temperature-responsive γ-Fe_2O_3-core/Au-shell nanoparticles (Au-mNPs) from diblock copolymer micelles. The amphiphilic diblock copolymer chains were synthesized using reversible addition fragmentation chain-transfer (RAFT) with a thermally-responsive "smart" poly(N-isopropylacrylamide) (pNIPAAm) block and an amine-containing poly(N,N-dimethylaminoethylacrylamide) (DMAEAm) block that acted as a reducing agent during gold shell formation. The Au-mNPs reversibly aggregated upon heating the solution above the transition temperature of pNIPAAm, resulting in a red-shifted localized surface plasmon resonance.

Keywords

RAFT polymer; localized surface plasmon resonance; core/shell nanoparticles; polymeric micelles; EDXS spectroscopy; stimuli-responsive nanoparticles

There has been increased interest in magnetic and metallic nanoparticles in the bionanotechnology field due to their potential in diagnostic and imaging technologies.[1–5] The microfluidics field in particular has offered opportunities to apply biofunctionalized nanoparticles in assays that are rapid yet highly sensitive in the detection of viral and bacterial pathogens, or antibodies to these pathogens, from biological fluids.[6–9] Such devices can potentially provide simultaneous detection of multiple conditions at the point-of-care.[10–12]

Thermally responsive polymers (e.g. pNIPAAm) have also been utilized with diagnostic reagents for assay technologies when conjugated to proteins13–18, and/or grafted to microfluidic device surfaces.19–25 These polymers enhance the capabilities of immunodiagnostic systems by separating and concentrating sample analytes from biological milleu through thermal aggregation and phase separation above their lower critical solution temperature (LCST). Magnetic nanoparticles represent a complementary separation technology in microfluidic systems that has been recently reviewed[26], and their thermally-responsive counterparts using pNIPAAm magnetic nanoparticles have been reported.27–33 When raised above the polymer LCST, the magnetic nanoparticles form particle aggregates with increased magnetophoretic mobility, resulting in faster separation in applied magnetic field gradients.[27, 29, 31, 33] Further developments in organic "smart"-polymer / inorganic-nanoparticle systems that combine stimuli-responsiveness with magnetic and optical properties could provide new opportunities for immunodiagnostic assay systems.

Dielectric-core gold-shell nanoparticles represent another inorganic material that has been used in bioassay and biomedical imaging due to their tunable plasmonic properties,34 surface

*Corresponding author. stayton@u.washington.edu.

properties,35 and the potential for surface-enhanced spectroscopies (e.g. surface-enhanced Raman scattering).[36] For example, silica-core gold-shell materials possess a tunable localized surface plasmon resonance (LSPR).34, 37 The LSPR wavelength can be tuned from the visible to the infrared based on the core:shell thickness ratio.38 Responsive polymers can be used to shift the LSPR of metallic nanoparticles through aggregation and near-field coupling.39–41

In an effort to streamline the synthesis of nanoparticles that combine the magnetic-core and gold-shell properties with the temperature-responsive properties of a pNIPAAm coating, we have developed a new strategy utilizing RAFT diblock copolymer chains. Previous approaches to magnetic-core gold-shell nanoparticle synthesis42–45 have relied on surface immobilization onto preformed magnetic cores (e.g. primary-amines or thiols), and subsequent reduction of ionic gold salts by an external reducing agent. Despite the recent success of these synthetic approaches, formation of small (<20 nm) magnetic-core gold-shell structures with a high degree of chemical functionality remains a challenge. Small nanoparticle sizes are highly desirable in diagnostic device applications where fast diffusion constants can decrease the interaction time required for efficient target capture at low analyte concentrations, resulting in faster and more sensitive assays.

Recent work has shown that certain secondary and tertiary amine-containing polymers are capable of acting as reducing agents,46–48 allowing for in-situ formation of gold nanoparticles displaying polymeric coronas.[49] Here we report that DMAEAm with a similar trialkyl amine residue is capable of acting as a reducing agent when polymerized as a diblock copolymer with pNIPAAm. The diblock copolymer architecture was designed so that the reducing amines are adjacent to a telechelic hydrocarbon tail contained in the RAFT chain transfer agent (CTA). Magnetic nanoparticles (mNPs) were then synthesized using these diblock copolymer micelles as dimensional confinements / stabilizing agents. The resultant mNPs retain the DMAEAm reducing moieties near the mNP surface, allowing for subsequent reduction of ionic gold salt (e.g. $HAuCl_4$ or $KAuCl_4$) onto the mNPs, forming a gold shell. This diblock copolymer-templated core / shell synthesis approach is depicted in Figure 1. Our new method for core-shell synthesis relies on distinct regions of polymeric functionality engineered through the chosen monomers, block lengths, and block sequence with respect to telechelic functional groups (e.g. $-C_{12}H_{25}$). Unlike previous approaches, no external reducing agent or metal-affinity ligands were required, as the chosen monomer (DMAEAm) served both these purposes, and the outer pNIPAAm block is incorporated at the time of initial core particle synthesis. The pNIPAAm block imparted colloidal stability and thermal-responsiveness that directs reversible nanoparticle aggregation.

Details on material suppliers and polymerization conditions can be found in the online Supplementary Information. The diblock copolymer was synthesized in two successive thermally initiated RAFT polymerizations, depicted in Figure 2. The product of the first polymerization was pNIPAAm ((i) in Figure 2) with $M_n \approx 15.9$ kDa, polydispersity (PDI) ≈ 1.14, degree of polymerization (dp_n) ≈ 141, as determined by size exclusion chromatography (SEC) (see Supplementary Information). The molecular weight of the pNIPAAm could be readily varied from 5 kDa-20 kDa by varying the ratio of NIPAAm:CTA in the feed solution, with PDI in the 1.1 range across all molecular weights investigated. Because of the heterobifunctionality of the CTA, the pNIPAAm displayed telechelic functional groups in the form of: (1) a dodecyl hydrocarbon tail, and (2) a carboxyl group, as shown in Figure 2. Poly (NIPAAm) is hydrophilic below its LCST (~32°C), and the presence of the hydrophobic $-C_{12}H_{25}$ tail directed these amphiphiles to form micelles in aqueous buffers and polar solvents (e.g. tetraglyme), as has been described previously for pNIPAAm displaying telechelic hydrocarbon tails.[31, 50]

The purified pNIPAAm material ((i) in Figure 2) was next used as a macro chain transfer agent (mCTA) for a second RAFT copolymerization of DMAEAm and NIPAAm (see Supplementary Information). This material is denoted as the amine-containing reducer diblock copolymer (ACR-dB; (ii) in Figure 2). The controlled living polymerization resulted in the insertion of DMAEAm and NIPAAm as a random copolymer between the hydrocarbon tail, and the homo-pNIPAAm block (Figure 2). This architecture allowed for localization of DMAEAm side-chains (Au-reduction moieties) adjacent to the micelle interior. ACR-dB preparations with pNIPAAm mCTA lengths of 15 and 5 kDa were prepared. In all cases, the feed ratio of DMAEAm:NIPAAm:mCTA in the second RAFT polymerization was maintained at 15:15:1. The resultant ACR-dB polymers had $M_n \approx 16$ kDa, PDI ≈ 1.25, and $M_n \approx 7.2$ kDa, PDI ≈ 1.25, respectively. ^{1}H-NMR and SEC characterization of the 5 and 15 kDa pNIPAAm, and the 7.2 kDa and 16 kDa ACR-dB, can be found in the Supplementary Information.

The amines from the DMAEAm-containing block served as electron donors in reducing ionic gold salts to form gold nanoparticles. Mixture of the polymer with $HAuCl_4$ or $KAuCl_4$ in alkaline buffers resulted in formation of gold nanoparticles (AuNPs) (Figure 3A, TEM), as has been reported for other tertiary-amine-containing polymers.[49] Thermally-responsive AuNPs (without magnetic cores) were formed by mixing 1.65 μmol (12 mg; 16.5 μmol DMAEAm reducing equilavents) of a 7.2 kDa ACR-dB with 23.8 μmol $HAuCl_4$ in 7 mL of DI water. The solution was kept in darkness at 22 °C for 24 hours, at which time 2.5 μmol of $HAuCl_4$ in 100 μL DI water was added. This solution was allowed to sit undisturbed for an additional 24 hours. The product was collected by 3 rounds of centrifugation (13.2 krpm, 5 minutes), and resuspended in DI water. As a control, a 5 kDa pNIPAAm mCTA ((i) in Figure 2) was mixed with the gold salt, and no characteristic pink color change was observed after 24–48 hours, as was the case for all ACR-dB preparations.

The resulting AuNPs formed with the 7.2 kDa ACR-dB were ~30–60 nm in diameter (Figure 3A, TEM), and exhibit spherical, triangular, and pentagonal shapes, depending on the gold concentrations used, and the timing of sequential addition of gold aliquots. The room temperature absorbance spectrum of the AuNPs showed LSPR bands at 540 nm and 685 nm (Supplementary Figure S2). The 685 nm absorbance peak was attributed to the triangular shaped particles.[51] Further studies are needed to improve homogeneity, and determine appropriate conditions for preferential formation of particular shapes. We note here that the pNIPAAm served as an excellent colloidal stabilizing agent for the AuNPs in solutions, which remained solubilized months stored at 4°C, or alternatively at room temperature in darkness.

The AuNPs display the pNIPAAm chains on the surface, and can aggregate at temperatures above the LCST. The LSPR of aggregated gold nanoparticles can undergo dramatic changes in resonance conditions due to dielectric coupling, giving rise to new plasmonic frequencies, and enhanced electric near-fields.[52, 53] Absorbance spectra were measured on a Hewlett Packard 8453 UV-Visible spectrophotometer with a temperature-controlled sample holder attached to a re-circulating heated waterbath. The sample temperature was raised at a rate of 1.2 °C/min, monitored using a digital thermocouple. We observed that both LSPR absorbance peaks (540 nm & 685 nm) of the AuNPs were red-shifted to longer wavelengths (Figure S2) upon heating the solution above the LCST of pNIPAAm. Typically the AuNP absorbance peaks were shifted 25–50 nm to the red upon raising the sample temperature above the LCST. These changes in the LSPR wavelength were partially reversible after cooling the solution to room temperature. More dilute solutions at lower pH (7 vs. 9) show weaker red-shifting with greater reversibility. A red-shifted LSPR has been previously reported in experimental data on nanoparticle aggregates,[54] and is also supported by theoretical modeling using Mie scattering and Maxwell-Garnett theory.55 Changes in the dielectric constant and refractive index due to the phase transition of the polymer chains at the surface of the AuNPs could also contribute to new resonance conditions.

After confirming that the DMAEAm side-chain could serve as an effective reducer of gold salts, we proceeded to use the diblock copolymer as a stabilizing agent in a micellar synthesis of magnetic nanoparticles (mNPs). The mNPs were synthesized using the method described previously by our group.[31] Briefly, 0.06 g of ACR-dB (M_n≈15.9 kDa) was dissolved (0.5 mM) in 7.5 mL of tetraglyme at 110 °C. 32 μL (0.2 mmol) of iron pentacarbonyl ($Fe(CO)_5$) was added to the solution, and the temperature was raised to 190 °C after 10 minutes of stirring. The solution was refluxed for 5 hours at 190 °C, and allowed to cool. The product (mNPs) was obtained by precipitation into pentane, re-dissolution in tetrahydrofuran, and thrice precipitation into pentane. The product was collected by centrifugation and dried overnight under vacuum. Further magnetic purification of the mNP material was undertaken (see Supplementary Information). A representative transmission electron micrograph (TEM) of the mNPs formed from the 15.9 kDa ACR-dB is shown in Figure 3B. The morphology of the mNPs is pseudo-spherical, with long axis diameter ≈ 10.4 ± 2.98 nm (mean ± std. dev.; # of particles counted ≥ 200).

In addition to its utility as a reducing agent, the DMAEAm monomer was chosen for its thermal stability. The more stable amide bond of DMAEAm prevents the side chains from being thermally degraded during the high-temperature (5 hours, 190 °C) mNP synthesis procedure. Monomers containing more labile ester bonds (e.g. dimethylaminoethylmethacrylate) were not suitable for retaining reducing moieties in high density at mNP surfaces.

Magnetometry characterization was performed using a superconducting quantum interference device (SQUID) with a field range of ± 5 T. The maximum magnetization reached was 54.2 and 69.11 emu/g γ-Fe_2O_3 at temperatures of 300 K, and 5 K, respectively (Supplementary Figure S3). The blocking temperature was found to be 22 K in the field-cooled curve (Supplementary Figure S4), similar to the previously published study.[31] In that study, SQUID magnetometry revealed a magnetic hysteresis, with a coercivity of 450 Oe.[31]

One advantage of our mNP synthesis procedure is that the mNPs as synthesized are soluble in water due to the hydrophilic nature of pNIPAAm below the LCST. The soluble mNPs in deionized water or PBS buffer (~15 mg/mL) had extremely low magnetophoretic mobility below the polymer LCST, and did not visibly respond to an applied magnetic field gradient in the form of a NdFeB magnet (5 cm × 1.27 cm × 0.63 cm, B_r max = 12.1 kilogauss) placed against the side of a 45 mL polypropylene tube. Above the LCST, however, the increased hydrophobicity of the pNIPAAm chains caused neighboring nanoparticles to aggregate. The aggregates exhibited magnetophoretic mobility that was much higher than the individual mNPs, so they were rapidly separated from solution using a permanent NdFeB magnet within minutes. This enhaned magnetophoretic mobility above the LCST was similar to that of the homo-pNIPAAm mNPs described previously.[31]

The DMAEAm group contained in the ACR-dB can be protonated with a formal positive charge below its pK_a of ~8, resulting in electrostatic repulsion between polymer chains. This imparted a pH-responsiveness to the mNP aggregation process, as demonstrated in Figure 4. When heated above the LCST, the degree of mNP aggregation was 2.7 times higher for mNPs dissolved in pH 8 vs. pH 7 (Figure 4). This finding is consistent with electrostatic repulsion hindering aggregate formation below the pK_a of the DMAEAm side-chains. Other groups have also reported that protonation of tertiary-amine co-monomers upon lowering the pH from 8 to 6 increases the LCST of pNIPAAm copolymers.[56] The pK_a of the DMAEAm monomer was estimated to be 8.8 by the Advanced Chemistry Development software package V8.14 for Solaris. Local environments could alter this predicted pK_a significantly for the polymeric form immobilized at the mNP surface.

Magnetic-core gold-shell nanoparticles were subsequently synthesized simply by mixing the mNP precursors with gold salts in alkaline buffers. Dissolution of 7.5 μmol of $KAuCl_4$ in 300 μL DI water was followed by addition of 1.3 mL of carbonate buffer (0.1 M, pH 10). To this, 1.5 mg of mNPs (synthesized with 15.9 kDa ACR-dB) in 150 μL DI water were added. The number of reducing DMAEAm equivalents was estimated at 1.8 μmol, based on SEC determined molecular weights (Supplementary Figure S1), and thermogravimetric analysis performed on a Perkin Elmer TGA7 instrument, which showed that the mNPs were 80% organic content by weight. The reaction proceeded in darkness at 22 °C for 36 hours. The product was obtained by magnetic enrichment with a permanent magnet (NdFeB, B_r max =12.1 kilogauss) at 45 °C (above the LCST of the polymer) for 15 minutes, followed by 24 hour dialysis against DI water. The resulting material consisted of a mixture of Au-mNP core-shell nanoparticles and nanoclusters, mNPs without gold, and very few AuNPs (without magnetic cores). Elemental compositions were confirmed using semi-quantitative energy dispersive x-ray spectroscopy (EDXS) in conjunction with high-resolution transmission electron microscopy (HR-TEM) (see below).

TEM (Figure 3) was performed on a Philips CM100 instrument with 100 kV accelerating voltage using a CCD camera (Gatan). In Figure 3C, 7.2 kDa ACR-dB / Au-mNPs are observed as high-contrast dark particles with semi-spherical and abnormal shapes. Unreacted mNPs without gold shells can be seen in Figure 3C as faint spots between the Au-mNPs. The higher electron density of gold makes Au-mNPs look darker in the electron micrograph as compared to the iron oxide mNPs. Polymer chains were not stained, and therefore were not observed in any of the TEM images.

The Au-mNP morphology was found to be dependent on concentration of the mNPs, and on the concentration and choice of chloroauric salt (e.g. $HAuCl_4$ or $KAuCl_4$). Heterogeneity of the resultant mixture was observed both in terms of mixtures of core-shell / un-reacted-core populations, as well as heterogeneity in shape of the core-shell population. Non-spherical core-shell structures were consistently observed (Figure 3C and Figure S7). Some resembled multiple particles that had fused together during gold reduction. The fusion of particles was more severe in the case of the Au-mNPs that were formed from mNPs displaying the 7.2 kDa ACR-dB, which had a higher ratio of DMAEAm:NIPAAm. Nanoparticles that appeared to have fused together during gold-shell formation were observed to form dimer, trimer, and elongated pearl necklace-like structures (see Supplementary Figure S7). This fusion is partially controlled by the concentration of mNPs and $KAuCl_4$, and by the ratio of DMAEAm:NIPAAm in the polymer preparation. These different aspect ratio Au-mNPs tended to broaden the LSPR, and in some cases a distinct NIR LSPR band above 600 nm was also observed. A magnetic purification step was employed in an attempt to ensure that all of the collected material exhibited some magnetic susceptibility. This purification step, however, did not remove un-reacted mNPs without gold (seen in Figure 3C as low contrast particles). Very few AuNPs (without magnetic cores) were also present in the mixture, formed possibly through reduction of the gold anion by the DMAEAm copolymer and subsequent diffusion away from the mNP surface, or by reduction in solution by free-polymer that had desorbed from the mNP surface. Since the AuNPs also displayed the thermally-responsive polymer groups, they were likely hydrophobically entrained and separated by mNPs and Au-mNPs during the magnetic purification step. The obtained material therefore consisted of a mixture of Au-mNPs, mNPs, and AuNPs.

During the Au-mNP formation reaction, the tertiary amine groups become positively charged through protonation or oxidation to an imine group.[57] These quaternary-amine compounds can chelate gold anions ($AuCl_4^-$) localizing them at the mNP surface, contributing to the growth of a cohesive shell. Cationic amine polymers have a demonstrated history as metal ion chelators, and dual reductants and stabilizers for formation of gold nanoparticles with diverse

morphology, and plasmonic properties.[58–61] Alkaline (pH 10) buffers were found to cause the reduction to occur more rapidly, with no observable color change at pH 4 after 48 hours. This suggests that it is the de-protonated tertiary-amines that act as the active reducing agent.

To confirm the elemental morphology of the core-shell Au-mNPs, HR-TEM imaging with semi-quantitative EDXS spectroscopy was used. A representative HR-TEM image of a single Au-mNP core-shell nanoparticle is shown in Figure 5A, with the corresponding EDXS spectrum shown in Figure 5B. All HR-TEM samples were analyzed on formvar coated / carbon-stabilized copper grids (Ted Pella) on a JEOL 2010 high-resolution TEM equipped with an Oxford ISIS X-ray EDXS microanalysis system. Nanoparticles were deposited by aerosolizing solutions onto the grid from deionized water. Semi-quantitative EDXS spectroscopy was performed by first acquiring a blank spectrum at locations on the grid very close (< 40 nm) to the nanoparticle to be analyzed. The circular illumination area of the electron beam was approximately 8–12 nm in diameter. The integrated Fe:Cu peak ratios were determined for the background samples of blank formvar. The Cu signal is observed due to scattered electrons impinging on the TEM grid away from the illumination area. The FeK α peak (6.21–6.7 keV) and the CuK β peak (8.61–9.29 keV) were integrated within the specified range, and their ratio was used to compare iron content between sampling volumes. Five blank samples were found to have an average Fe:Cu integrated peak ratio of 0.123 ± 0.007 (mean ± s.d.). The Au-mNP was then imaged and the nanoparticle EDXS spectrum was collected to determine the Fe:Cu. For the Au-mNP shown in Figure 5A, the Fe:Cu ratio was found to be 0.199, representing 10.8 standard deviations above the background mean. We note that we have not performed k-factor analysis, nor have we corrected for absorption processes as is necessary particularly when trying to quantify a light element inside a heavier elemental matrix.[62] However, we conclude from our analysis that Fe was present in the illumination volume. The signal for gold meanwhile remained strong throughout all EDXS spectra where the electron dense / high contrast material is observed. These results confirmed that both elements (Fe and Au) were co-localized in single nanoparticles. This technique allowed us to confirm that core-shell Au-mNPs, mNPs, and very few AuNPs were all present in samples. The ratio of low-contrast mNPs to high-contrast Au-containing particles was ~1:1.25, based on TEM image analysis (# particles counted > 500). See Supplementary Information for HR-TEM and EDXS of mNPs and AuNPs.

The Au-mNPs were found to have a LSPR wavelength of 525 nm at room temperature in pH 8 PBS buffer (Figure 6, solid line). Due to the pNIPAAm on the particle surface, the LSPR absorbance bands of the Au-mNPs shifted with temperature. Upon raising the temperature to 45 °C (Figure 6, dashed line), the LSPR was found to have shifted to 560 nm. Cooling the solution back to room temperature resulted in a blue-shift of the LSPR to 545 nm. As the particles began to aggregate, the amount of light scattered from the solution increased, decreasing the total amount of light that reached the detector across all wavelengths. This explains the rising baseline seen in Figure 6 (the spectra are not offset).

In summary, we have demonstrated how RAFT polymerization can be used to engineer amphiphilic organic diblock copolymer chains capable of templating inorganic magnetic-core gold-shell nanoparticle compositions. A $-C_{12}H_{25}$ hydrocarbon tail drives formation of micelles, which are loaded with a hydrophobic organometallic iron compound that thermally decomposes in the interior of the micelle. The amine-containing monomer (DMAEAm) displayed near the mNP surface is capable of reducing gold salts forming metallic shells that support LSPR oscillations. The material is heterogeneous and partially consisted of Au-mNP core-shell nanoparticles and nanoclusters. Further work is being performed to acquire homogeneous populations. An advantage of our approach is that the same polymer was used for synthesis of AuNPs, mNPs, and Au-mNPs, all exhibiting temperature-responsive properties. Reversible aggregation and plasmonic behavior of the AuNPs, and Au-mNPs was described, and future work will focus on application of these particles in Au-mNP-based

bioassays relying on spectroscopic detection methods (e.g. SERS) that utilize the enhanced magnetic and plasmonic properties demonstrated herein.

Supplementary Material

Refer to Web version on PubMed Central for supplementary material.

Acknowledgments

Michael A. Nash acknowledges funding from the National Science Foundation Graduate Research Fellowship Program (NSF-GRFP), and from the U.S. Department of Homeland Security (DHS) Scholarship and Fellowship Program, administered by the Oak Ridge Institute for Science and Education (ORISE) through an interagency agreement between the U.S. Department of Energy (DOE) and DHS. A portion of this research was performed at EMSL, a national scientific user facility sponsored by the Department of Energy's Office of Biological and Environmental Research located at Pacific Northwest National Laboratory. The authors express gratitude to the NIH (Grant EB000252) and to the Bill and Melinda Gates Foundation Grand Challenges Program for funding.

References

1. Georganopoulou DG, Chang L, Nam JM, Thaxton CS, Mufson EJ, Klein WL, Mirkin CA. Proceedings of the National Academy of Sciences of the United States of America 2005;102(7):2273–2276. [PubMed: 15695586]
2. Lin AWH, Lewinski NA, West JL, Halas NJ, Drezek RA. Journal of Biomedical Optics 2005;10(6)
3. Loo C, Lowery A, Halas N, West J, Drezek R. Nano Letters 2005;5(4):709–711. [PubMed: 15826113]
4. Storhoff JJ, Lucas AD, Garimella V, Bao YP, Muller UR. Nature Biotechnology 2004;22(7):883–887.
5. Veiseh O, Sun C, Gunn J, Kohler N, Gabikian P, Lee D, Bhattarai N, Ellenbogen R, Sze R, Hallahan A, Olson J, Zhang MQ. Nano Letters 2005;5(6):1003–1008. [PubMed: 15943433]
6. Hahn YK, Jin Z, Kang JH, Oh E, Han MK, Kim HS, Jang JT, Lee JH, Cheon J, Kim SH, Park HS, Park JK. Analytical Chemistry 2007;79(6):2214–2220. [PubMed: 17288405]
7. Lacharme F, Vandevyver C, Gijs MAM. Analytical Chemistry 2008;80(8):2905–2910. [PubMed: 18348542]
8. Kim KS, Park JK. Lab on a Chip 2005;5(6):657–664. [PubMed: 15915258]
9. Luo CX, Fu Q, Li H, Xu LP, Sun MH, Ouyang Q, Chen Y, Ji H. Lab on a Chip 2005;5(7):726–729. [PubMed: 15970965]
10. Yager P, Edwards T, Fu E, Helton K, Nelson K, Tam MR, Weigl BH. Nature 2006;442(7101):412–418. [PubMed: 16871209]
11. Yager P, Domingo GJ, Gerdes J. Annual Review of Biomedical Engineering 2008;10:107–144.
12. Nelson KE, Foley JO, Yager P. Analytical Chemistry 2007;79(10):3542–3548. [PubMed: 17437332]
13. Auditorehargreaves K, Houghton RL, Monji N, Priest JH, Hoffman AS, Nowinski RC. Clinical Chemistry 1987;33(9):1509–1516. [PubMed: 3304710]
14. Ding ZL, Long CJ, Hayashi Y, Bulmus EV, Hoffman AS, Stayton PS. Bioconjugate Chemistry 1999;10(3):395–400. [PubMed: 10346869]
15. Hoffman AS. Clinical Chemistry 2000;46(9):1478–1486. [PubMed: 10973893]
16. Takei YG, Aoki T, Sanui K, Ogata N, Okano T, Sakurai Y. Bioconjugate Chemistry 1993;4(1):42–46. [PubMed: 8431511]
17. Takei YG, Aoki T, Sanui K, Ogata N, Okano T, Sakurai Y. Bioconjugate Chemistry 1993;4(5):341–346. [PubMed: 8274517]
18. Takei YG, Matsukata M, Aoki T, Sanui K, Ogata N, Kikuchi A, Sakurai Y, Okano T. Bioconjugate Chemistry 1994;5(6):577–582. [PubMed: 7873660]
19. Ebara M, Hoffman JM, Hoffman AS, Stayton PS. Lab on a Chip 2006;6(7):843–848. [PubMed: 16804587]
20. Ebara M, Hoffman JM, Stayton PS, Hoffman AS. Radiation Physics and Chemistry 2007;76(8–9):1409–1413.

21. Kanazawa H, Nishikawa M, Mizutani A, Sakamoto C, Morita-Murase Y, Nagata Y, Kikuchi A, Okano T. Journal of Chromatography A 2008;1191(1–2):157–161. [PubMed: 18289554]
22. Malmstadt N, Hoffman AS, Stayton PS. Lab on a Chip 2004;4(4):412–415. [PubMed: 15269814]
23. Malmstadt N, Hyre DE, Ding ZL, Hoffman AS, Stayton PS. Bioconjugate Chemistry 2003;14(3): 575–580. [PubMed: 12757381]
24. Malmstadt N, Yager P, Hoffman AS, Stayton PS. Analytical Chemistry 2003;75(13):2943–2949. [PubMed: 12964737]
25. Nagase K, Kobayashi J, Kikuchi AI, Akiyama Y, Kanazawa H, Okano T. Langmuir 2008;24(2):511–517. [PubMed: 18085801]
26. Gijs MAM. Microfluidics and Nanofluidics 2004;1(1):22–40.
27. Furukawa H, Shimojyo R, Ohnishi N, Fukuda H, Kondo A. Applied Microbiology and Biotechnology 2003;62(5–6):478–483. [PubMed: 12750854]
28. Narain R, Gonzales M, Hoffman AS, Stayton PS, Krishnan KM. Langmuir 2007;23(11):6299–6304. [PubMed: 17451262]
29. Sun YB, Ding XB, Zheng ZH, Cheng X, Hu XH, Peng YX. Chemical Communications 2006;26:2765–2767. [PubMed: 17009456]
30. Wakamatsu H, Yamamoto K, Nakao A, Aoyagi T. Journal of Magnetism and Magnetic Materials 2006;302(2):327–333.
31. Lai JJ, Hoffman JM, Ebara M, Hoffman AS, Estournes C, Wattiaux A, Stayton PS. Langmuir 2007;23 (13):7385–7391. [PubMed: 17503854]
32. Wuang SC, Neoh KG, Kang ET, Pack DW, Leckband DE. Advanced Functional Materials 2006;16 (13):1723–1730.
33. Lai JJ, Nelson KE, Nash MA, Hoffman AS, Yager P, Stayton PS. Lab on a Chip. 2009 (in press).
34. Oldenburg SJ, Averitt RD, Westcott SL, Halas NJ. Chemical Physics Letters 1998;288(2–4):243–247.
35. Pourbaix M. Biomaterials 1984;5(3):122–134. [PubMed: 6375748]
36. Oldenburg SJ, Westcott SL, Averitt RD, Halas NJ. Journal of Chemical Physics 1999;111(10):4729–4735.
37. Westcott SL, Oldenburg SJ, Lee TR, Halas NJ. Langmuir 1998;14(19):5396–5401.
38. Westcott SL, Oldenburg SJ, Lee TR, Halas NJ. Chemical Physics Letters 1999;300(5–6):651–655.
39. Zhu MQ, Wang LQ, Exarhos GJ, Li ADQ. Journal of the American Chemical Society 2004;126(9): 2656–2657. [PubMed: 14995155]
40. Yusa SI, Fukuda K, Yamamoto T, Iwasaki Y, Watanabe A, Akiyoshi K, Morishima Y. Langmuir 2007;23(26):12842–12848. [PubMed: 17994778]
41. Raula J, Shan J, Nuopponen M, Niskanen A, Jiang H, Kauppinen EI, Tenhu H. Langmuir 2003;19 (8):3499–3504.
42. Xu ZC, Hou YL, Sun SH. Journal of the American Chemical Society 2007;129(28) 8698-+
43. Lim JK, Tilton RD, Eggeman A, Majetich SA. Journal of Magnetism and Magnetic Materials 2007;311(1):78–83.
44. Ji XJ, Shao RP, Elliott AM, Stafford RJ, Esparza-Coss E, Bankson JA, Liang G, Luo ZP, Park K, Markert JT, Li C. Journal of Physical Chemistry C 2007;111(17):6245–6251.
45. Lyon JL, Fleming DA, Stone MB, Schiffer P, Williams ME. Nano Letters 2004;4(4):719–723.
46. Richardson MJ, Johnston JH, Borrmann T. European Journal of Inorganic Chemistry 2006;13:2618–2623.
47. Newman JDS, Blanchard GJ. Langmuir 2006;22(13):5882–5887. [PubMed: 16768524]
48. Chatterjee U, Jewrajka SK. Journal of Colloid and Interface Science 2007;313(2):717–723. [PubMed: 17574566]
49. Li YT, Smith AE, Lokitz BS, McCormick CL. Macromolecules 2007;40(24):8524–8526.
50. Kujawa P, Segui F, Shaban S, Diab C, Okada Y, Tanaka F, Winnik FM. Macromolecules 2006;39 (1):341–348.
51. Jin RC, Cao YC, Hao EC, Metraux GS, Schatz GC, Mirkin CA. Nature 2003;425(6957):487–490. [PubMed: 14523440]

52. Jain PK, Huang WY, El-Sayed MA. Nano Letters 2007;7(7):2080–2088.
53. Storhoff JJ, Lazarides AA, Mucic RC, Mirkin CA, Letsinger RL, Schatz GC. Journal of the American Chemical Society 2000;122(19):4640–4650.
54. Kneipp K, Kneipp H, Itzkan I, Dasari RR, Feld MS. Journal of Physics-Condensed Matter 2002;14 (18):R597–R624.
55. Ghosh SK, Pal T. Chemical Reviews 2007;107(11):4797–4862. [PubMed: 17999554]
56. Feil H, Bae YH, Jan FJ, Kim SW. Macromolecules 1993;26(10):2496–2500.
57. Lee KY, Hwang J, Lee YW, Kim J, Han SW. Journal of Colloid and Interface Science 2007;316(2): 476–481. [PubMed: 17727872]
58. Shi XY, Sun K, Baker JR. Journal of Physical Chemistry C 2008;112(22):8251–8258.
59. Sardar R, Park JW, Shumaker-Parry JS. Langmuir 2007;23(23):11883–11889. [PubMed: 17918982]
60. Kuo PL, Chen CC, Jao MW. Journal of Physical Chemistry B 2005;109(19):9445–9450.
61. Chen CC, Hsu CH, Kuo PL. Langmuir 2007;23(12):6801–6806. [PubMed: 17480111]
62. Brydson, R. Electron energy-loss spectroscopy and energy dispersive X-ray analysis Ch. 4 in Nanocharacterisation. Cambridge: Royal Society of Chemistry; 2007.
63. Moad G, Chong YK, Postma A, Rizzardo E, Thang SH. Polymer 2005;46(19):8458–8468.

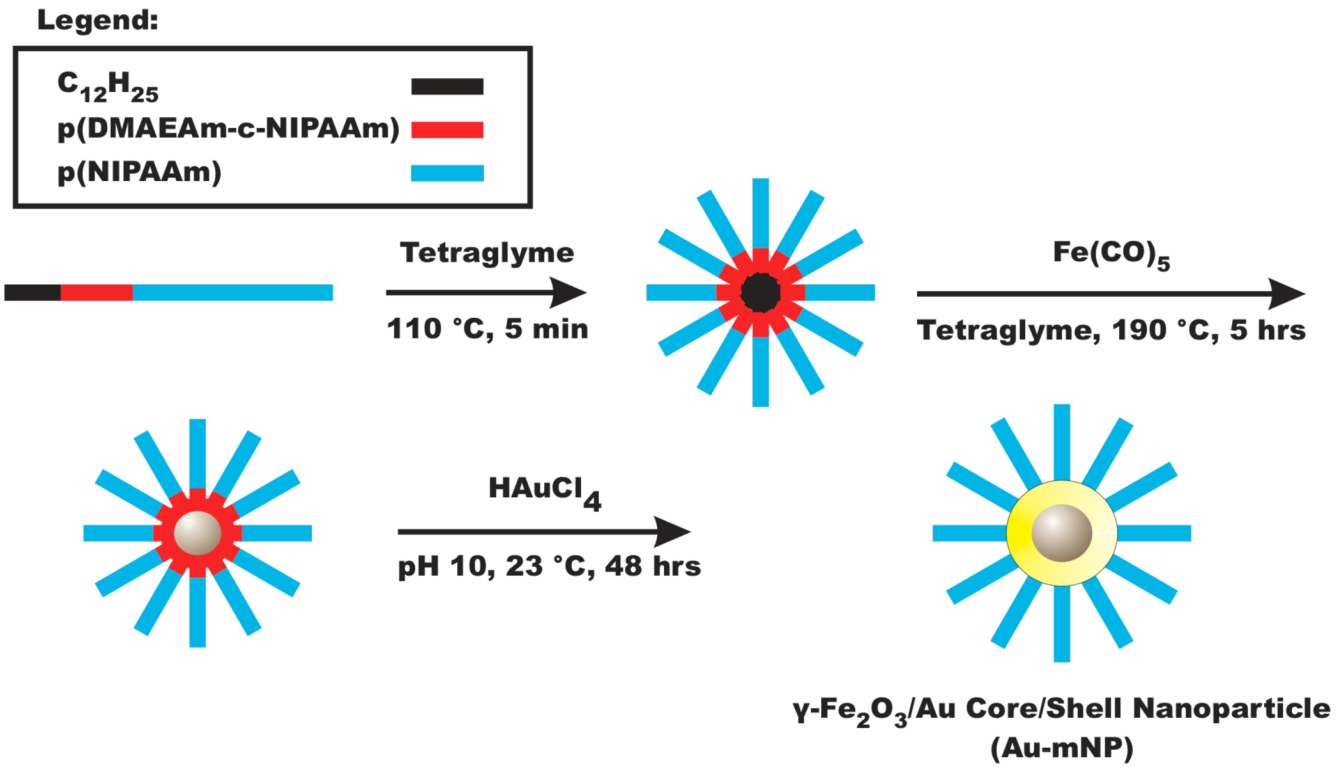

Figure 1.

Magnetic-core gold-shell nanoparticle synthesis scheme. Amphiphilic diblock copolymers were designed with a dodecyl hydrocarbon tail (black), an amine-containing reducer (ACR) block (red), and a thermally-responsive homo-pNIPAAm block (blue). These polymers form micelles, which are used as nanoscale reactors for magnetic nanoparticle (mNP) synthesis from iron pentacarbonyl precursors. The mNPs retain the DMAEAm reducing moieties at the nanoparticle surface, allowing for subsequent reduction and formation of a gold shell on the mNP core.

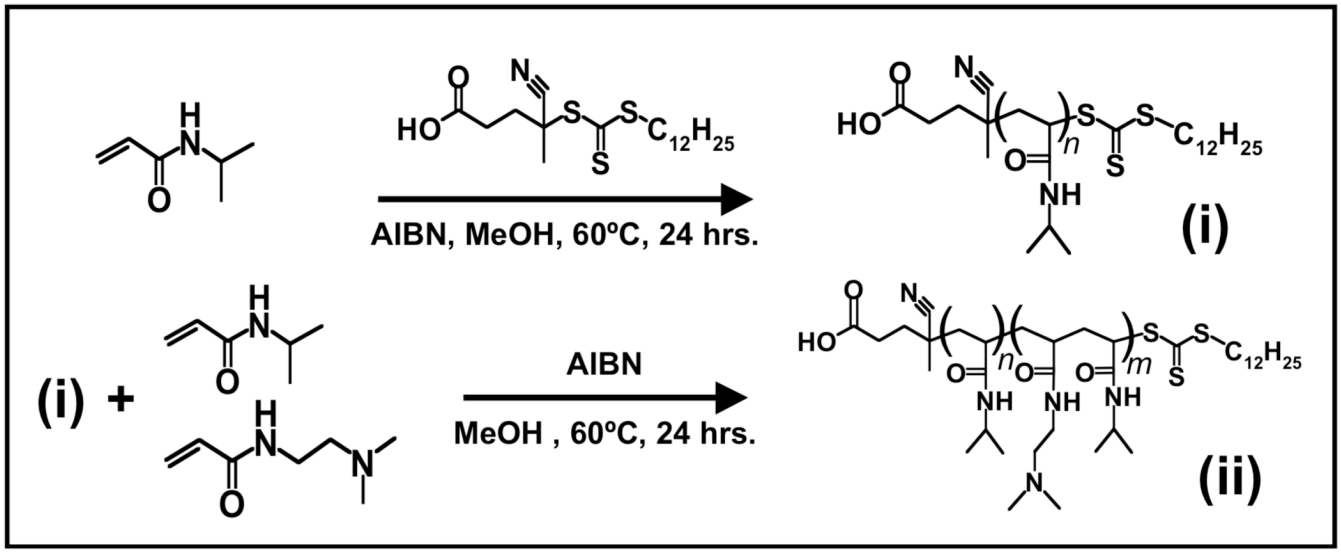

Figure 2.

Polymer synthesis scheme. RAFT polymerization was carried out in two sequential reactions. In the first, the RAFT chain transfer agent (CTA) facilitates polymerization of NIPAAm while maintaining telechelic functional groups, forming the homo-pNIPAAm macro-CTA (mCTA, (i)). mCTA molecular weights investigated were 5, and 15 kDa. The mCTA was purified and reacted similarly with a mixture of DMAEAm and NIPAAm, producing the amine-containing reducer diblock (ACR-dB, (ii)).

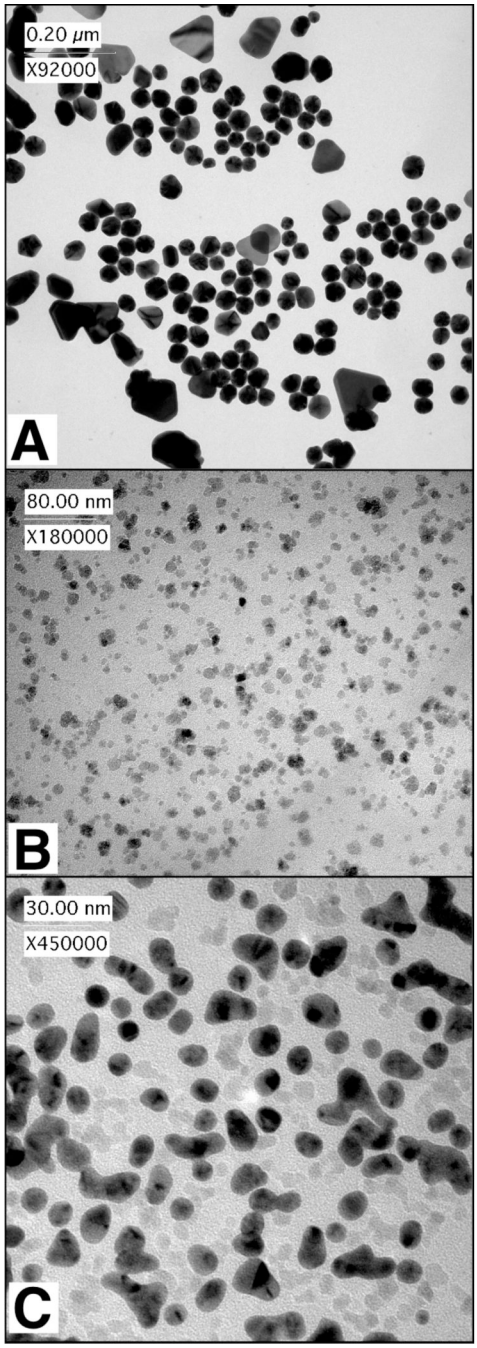

Figure 3.
Representative TEM images of nanoparticle compositions. (A) Gold nanoparticles (AuNPs) were formed by mixing the ACR-dB (M_n 7.2 kDa) with $HAuCl_4$ in deionized water. (B) Magnetic nanoparticles (mNPs) were synthesized from $Fe(CO)_5$ and ACR-dB (M_n 16 kDa) in tetraglyme. (C) Magnetic-core / gold-shell nanoparticles (Au-mNPs) were formed through aqueous reaction of mNPs (7.2 kDa) with $KAuCl_4$.

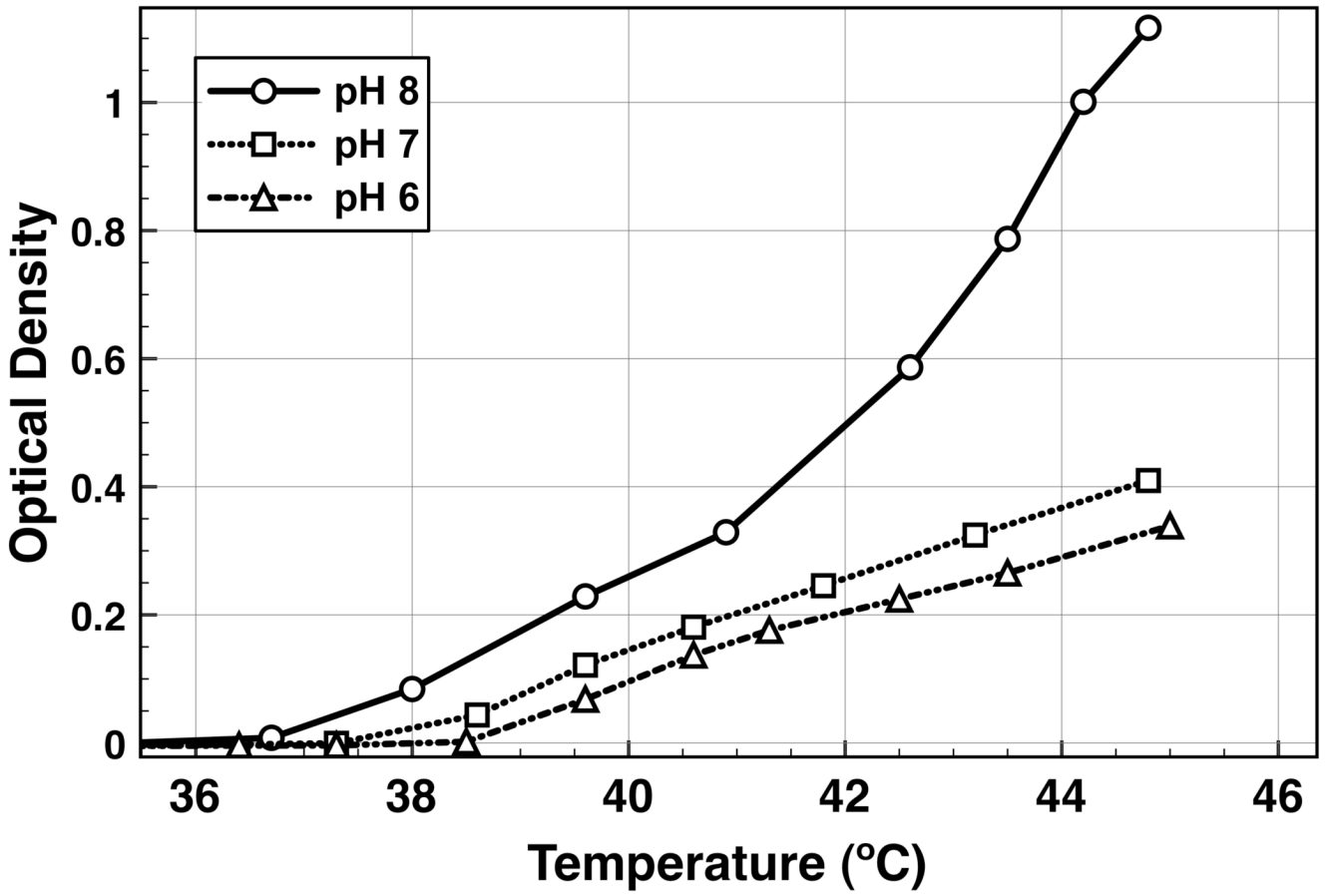

Figure 4.
pH response of mNP light scattering as a function of temperature. Optical density at 650 nm was measured for mNPs (1 mg/mL) at pH 6 (triangles), 7 (squares), and 8 (circles) in PBS buffer as the solution temperature was raised at 1.2 °C/min.

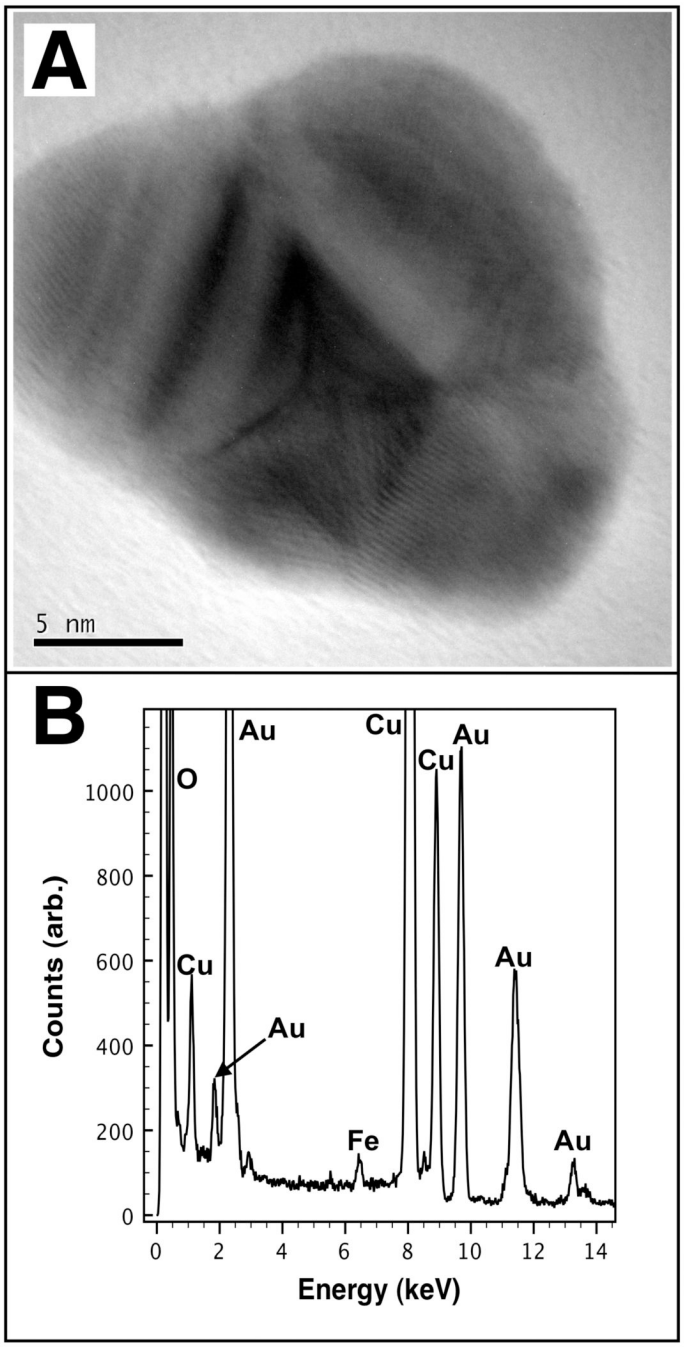

Figure 5.
HR-TEM and EDXS spectrum of a single core/shell Au-mNP. (A) HR-TEM image of the AumNP. (B) EDXS spectrum of the Au-mNP shown in (A). Copper is observed due to the TEM grid.

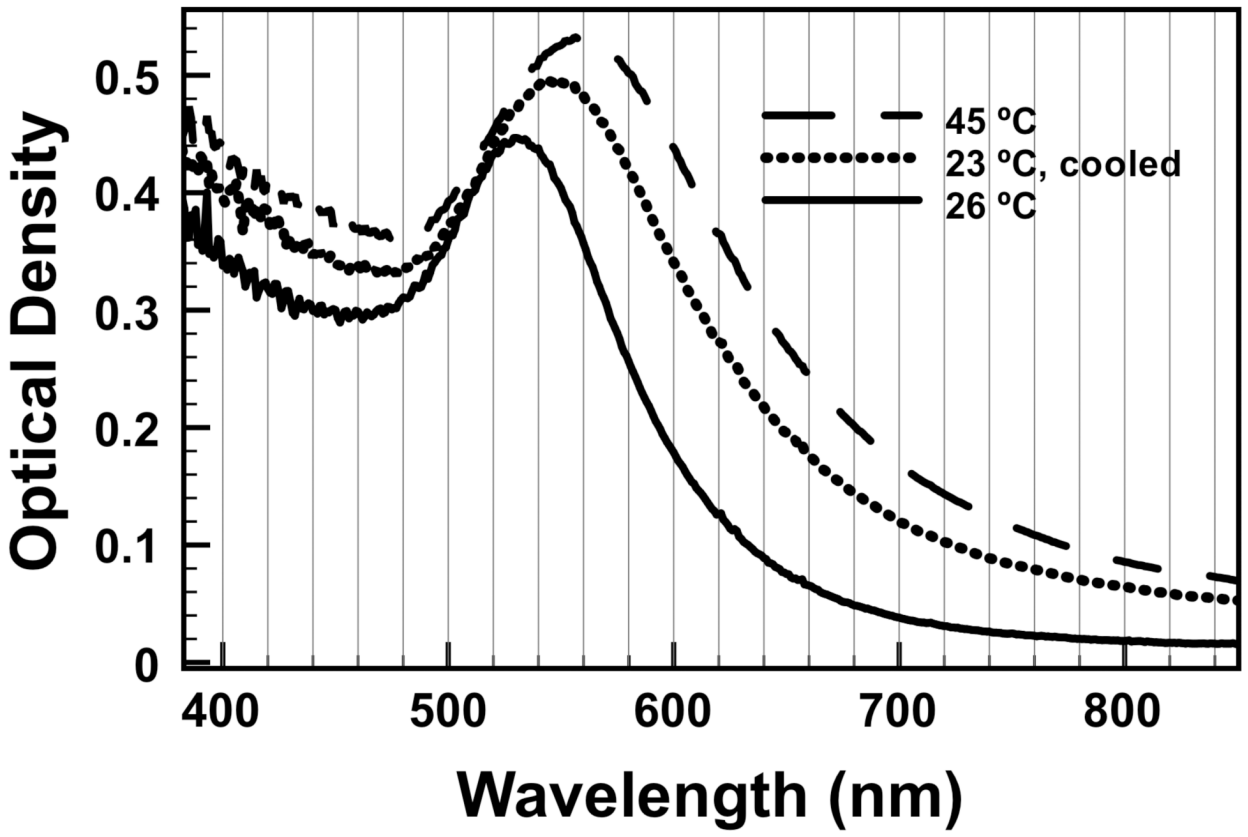

Figure 6.
Absorbance spectrum of Au-mNPs as a function of temperature. The absorbance spectrum for 7.2 kDa Au-mNPs dissolved in pH 8 PBS was taken at room temperature (solid line), 45 °C (dashed line), and cooled from 45 °C back to 23 °C (dotted line).